A perspective on Diamond MEMS magnetic sensors

Zilong Zhang[1, 2], Keyun Gu[1], Masaya Toda[2], and Meiyong Liao[1 *]

[1] Research Center for Electronic and Optical Materials, National Institute for Materials Science (NIMS), Tsukuba, Ibaraki, Japan

[2] Graduate School of Engineering, Tohoku University, Sendai, Miyagi 9808579, Japan

Correspondence should be addressed to Meiyong Liao* (Email: meiyong.liao@nims.go.jp)

ABSTRACT

Microelectromechanical system (MEMS) has unlocked a wide range of applications in electronics, mobility, medical and energy from sensors and actuators to switches. Diamond, in particular, stands out for its exceptional mechanical robustness and electronic performance in extreme conditions, offering sensitivity and reliability super to other semiconductor materials for MEMS sensors. In this perspective, we review the principles of MEMS magnetic sensors, diamond for MEMS, thermal stability of diamond MEMS resonators, and diamond MEMS magnetic sensors, particularly for the applications under high temperatures. We present the interface engineering of diamond MEMS magnetic sensors to improve the thermal stability. Finally, we discuss the potential solutions, outline future research directions, and discuss the prospects for continued progress of diamond MEMS.

I. INTRODUCTION

Magnetic sensors have become increasingly vital in modern applications, including automotive sensors, navigation systems, non-contact sensing, biomedical devices, and nondestructive testing etc.[1-3]. Currently, the most common types of magnetic sensors include superconducting quantum interference devices (SQUID), fluxgate sensors, Hall sensors, giant magnetoresistance (GMR) sensors, and micro-electromechanical systems (MEMS) magnetic sensors, etc.[1-5] Although these magnetic sensors have been widely applied in either industry, daily life, aerospace and scientific research, the development of alternative magnetic sensors are still in demand to overcome the limitations of each kind of sensors, i.e. the low-temperature requirement of SQUID devices a, low sensitivity of Hall sensors, high-power consumption of fluxgate sensors, and poor thermal stability of GMR sensors.[2,6] In contrast, MEMS magnetic sensors offer several advantages, including microscale size, batch manufacturing, low-power consumption, high sensitivity and resolution, and smart system integration with CMOS technology.[2] Silicon based MEMS has experienced explosive growth due to the maturity in micromachining and CMOS process. Next-generation MEMS devices are expected to be more precise, highly reliable and entering from the classic sensors to quantum field.

Diamond with an ultra-wide bandgap energy, exceptional electronic, mechanical, and thermal properties, has been extensively investigated as the next-generation semiconductors not only for conventional electronics superior to the other semiconductors, but also for high-performance and high-reliability MEMS devices. The high quality *(Q)* factor over 1 million at room temperature and the thermal stability up to 500^{o}C based on single-crystal diamond (SCD) MEMS cantilevers were demonstrated.[7,8]

This Perspective aims to furnish a brief overview of the latest research and discuss

challenges and opportunities of SCD MEMS magnetic sensors for extreme conditions. We provide a brief introduction of the principles of MEMS resonant-type magnetic sensors and show the merits of diamond for MEMS applications. We then present the diamond MEMS magnetic sensors operable up to 500ºC. We explore the interface engineering to improve either the sensitivity and reliability of the diamond MEMS magnetic sensors. We summarize the recent advance in this field and discuss the future roadmap of diamond MEMS magnetic sensors. Section II introduces intrinsic material properties, highlighting various SCD MEMS fabrication techniques of diamond MEMS. Section III provides a device concept and recent advance of SCD MEMS in high-temperature magnetic sensing. Section IV outlines the challenges and opportunities ahead. By reviewing the current state of the field and highlighting potential research directions, this paper seeks to provide valuable insights and inspire future work in this growing area.

II. MEMS RESONANT MAGNETIC SENSORS

MEMS resonant magnetic sensors are designed to detect magnetic fields by leveraging changes in resonance frequency. These sensors exploit the interaction between magnetic fields and mechanical structures, which causes change in the resonance of the sensor's mechanical components. In general, the sensor consists of a resonant structure, such as a cantilever beam, a double-clamped beam, or a membrane, etc, which is subjected to magnetic forces when exposed to a magnetic field. These forces cause mechanical deformation or vibration in the structure, altering its resonance frequency. The magnetic field is then quantified by measuring these resonance frequency shifts. The principles underlying MEMS resonant magnetic sensing can be mainly categorized into the following types: (1) Lorentz force principle,[9-14] (2) ΔE effect, which is based on the

magnetostrictive effect,[5,15-20] (3) magnetoelectric effect,[21-23] (4) torque effect,[24,25] and (5) magnetic gradient effect.[26] The Lorentz force principle need a conductive component on the MEMS structure, in which the electric current flows. The interaction between the current and the field generates a Lorentz force on the conductor. In MEMS devices, this force induces mechanical displacement, altering the system's resonant frequency. By accurately measuring these frequency shifts, the sensor can determine the strength of the magnetic field.[9-14] The ΔE effect, a manifestation of the magnetostrictive effect, underpins the operation of many high-performance MEMS resonance magnetic sensors. For materials with magnetostrictive properties, such as FeGa, the Young's modulus changes when subjected to an external magnetic field. This variation in stiffness directly influences the resonant frequency of the MEMS device, where the frequency shift is proportional to the intensity of the magnetic field.[5,15-20] This sensing mechanism is particularly advantageous in applications requiring dynamic field detection. The magnetoelectric (ME) effect, involves the interaction between magnetic fields and electric polarization in multiferroic or composite materials. In MEMS resonance sensors, this effect is achieved by creating strain in the piezoelectric material generated in the magnetrostrictive material. This strain generates an electric field which can be enhanced at the MEMS sensor's resonant frequency.[21-23] This coupling provides a highly sensitive method for converting magnetic field variations into measurable electrical signals, making it ideal for compact, energy-efficient sensing applications. The torque effect in MEMS magnetic sensors occurs when a magnetic element or dipole within the sensor interacts with an external magnetic field. The external field exerts a torque on the magnetic dipole, resulting in mechanical rotation or bending of the MEMS structure. In cantilever-based sensors, this torque produces a twisting force that shifts the resonator's

resonant frequency. By measuring the changes in resonance caused by the torque, the sensor can detect the magnetic field's magnitude and direction.[24,25] This principle is particularly valuable in applications requiring precise directional sensing of magnetic fields. The magnetic gradient effect is employed in MEMS sensors to detect spatial variations in magnetic fields. When the magnetic field is non-uniform, different parts of the sensor experience varying magnetic forces, creating a mechanical response. This differential force distribution induces changes in the resonant behavior of the MEMS structure. By analyzing these changes, the sensor can measure the magnetic field gradient, which is the rate of change of the magnetic field over a given distance. [26] This principle is often used in magnetic gradiometers for applications requiring high spatial resolution, such as detecting localized magnetic sources or performing fine-scale magnetic mapping.

Especially, the ΔE effect, has aroused great attention to develop MEMS resonant magnetic sensors with exceptional sensitivity to low frequencies and low magnetic fields and high integration.[17,27-30]. The MEMS magnetic sensors based on the ΔE effect is the preferred solution for certain specific applications under extreme conditions.[8,31,32] By optimizing device structure and selecting appropriate ferromagnetic materials, the performance such as the sensitivity, resolution, response time and reliability of the MEMS magnetic sensors based ΔE effect can be tuned.

III. DIAMOND MEMS

A. Overview of diamond MEMS

Micro- and nano-electromechanical systems (MEMS/NEMS) represent an advanced interdisciplinary field that integrates electrical and mechanical components. Due to their compact size, high sensitivity, low power consumption, and compatibility with modern electronics, these devices are highly promising for applications in automation, industry,

edge computing, augmented and virtual reality, biomedicine, telecommunications, and quantum mechanics.[33,34] A high product of frequency and quality (Q) factor are desirable in many cases for achieving high sensitivity, high resolution, and high speed.[35,36] However, the inherent limitations of silicon, including its narrow bandgap, prone to oxidation, and mechanical brittleness, especially at the nanoscale, have limited the performance, such as sensitivity, precision, and reliability of current MEMS devices.

Wide-bandgap semiconductors like SiC, GaN, AlN, and diamond are considered promising for MEMS applications. Among these semiconductors, diamond stands out as an ideal choice due to its exceptional electrical properties, mechanical strength, and chemical resistance in harsh environments.[37] **Fig. 1** summarizes the superlative properties of diamond materials, such as high Young's modulus, compressive strength, the highest mechanical hardness and low coefficient of friction, compared with other semiconductors. The superior tribological properties of diamond ensure that its wear lifetime is 10,000 times greater than that of silicon, enhancing the reliability of MEMS devices. Additionally, diamond has low inherent losses, such as those from thermoelastic damping, leading to MEMS devices with higher Q factors.[38] **Fig. 2** compares and summarizes the resonance frequencies and Q factors, and the fQ product of the representative MEMS resonators based on various semiconductors. It is disclosed that the as-fabricated diamond MEMS resonators can achieve higher Q factors than those of other semiconductors **(Fig. 2(a))**. In addition, for a certain resonance frequency, the product fQ of diamond is higher than other materials **(Fig. 2(b))**. Diamond's chemical inertness means that its surface remains free of natural solid oxides, minimizing the surface loss in MEMS devices. Its wide bandgap and high resistance to radiation further ensure stable performance in harsh conditions. Consequently, diamond stands out as an ideal material for MEMS

applications.[39,40]

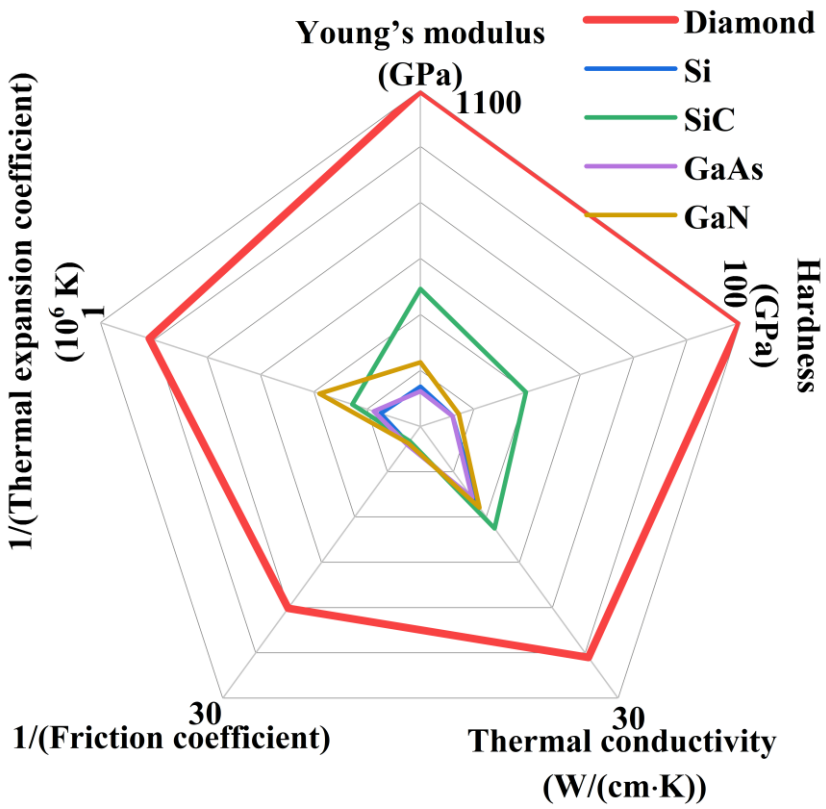

FIG. 1. Comparison of mechanical material properties of various semiconductors.[41-47]

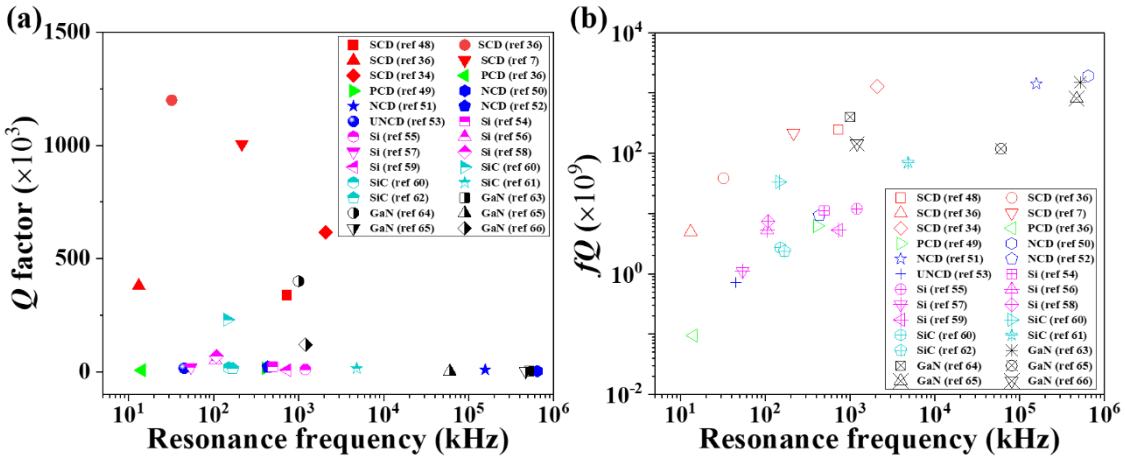

FIG. 2. Comparisons of (a) resonance frequencies, f and Q factors and (b) the product of f and Q, fQ of representative MEMS resonators made from various semiconductors.[7,34,36,48-66]

Polycrystalline diamonds, including microcrystalline, nanocrystalline, and

ultrananocrystalline varieties have been explored for MEMS and exciting proto-type MEMS devices were reported.[42,53] These materials have numerous grain boundaries and impurities, leading to increased internal losses and limiting the resonance performance.[67] Compared to these above-mentioned diamonds, SCD can make full use of the ultimate properties of diamond material in every aspect for MEMS applications with high performance and high reliability, especially under extreme conditions. SCD MEMS can be employed in classic sensing, actuator and switch applications[68] as well as photonic devices.[69,70] We briefly summarize the development of SCD MEMS technology in **Fig. 3**.

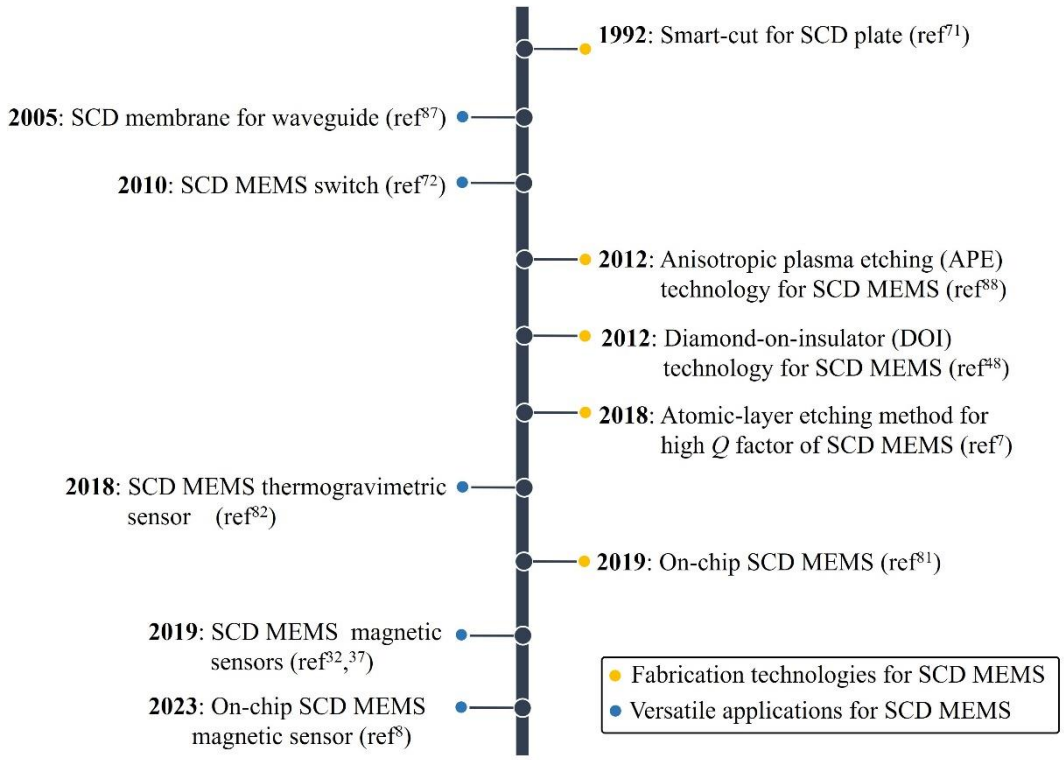

FIG. 3. Development timeline of SCD MEMS technology.[7,8,32,37,48,71-73,81,82,87,88]

Note that Fig. 3 does not includes the technology like embedding diamond nanowire as a tip on a silicon cantilever. Based on the smart-cut method for SCD plate,[71] SCD membrane[87] was created and the first device concept of SCD MEMS with movable

cantilever beams in a electromechanical switch configuration was reported in 2010.[72] The smart-cut process enables mass production of SCD MEMS/NEMS structures with high controllability and reproducibility and thus the development of SCD MEMS magnetic sensors capable of working at high temperatures.[8,31,32,37,73] The reported applications of SCD MEMS are summarized in **Fig. 4**, such as capacitive pressure sensors,[74] atomic force microscopy,[75-77] actuators,[78] and NV center magnetic imaging sensors.[79,80] Particularly, the SCD MEMS was used for high-temperature magnetic sensors,[8,32,37] switch,[72] temperature sensor,[81] and thermogravimetric sensor.[82] In addition, the SCD MEMS photonics applications, such as waveguides, photonic crystals, and optical micro-nano resonators,[83,84] have significantly advanced the field of cavity optomechanics.[85,86]

FIG. 4. Developed SCD MEMS/NEMS devices for general conditions and extreme

conditions. Reprinted with permission from Fu *et al*., Sci. Rep. 9 (1), 1 (2019). Copyright 2019 Springer Nature Limited,[74] Tao *et al*., Nano Lett. 15 (12), 7893 (2015). Copyright 2015 American Chemical Society,[77] Liao *et al*., Adv. Sci. 11 (13), 2306013 (2024). Copyright 2024 Wiley-VCH GmbH,[78] Appel *et al*., Rev. Sci. Instrum. 87 (6), 063703 (2016). Copyright 2016 AIP Publishing LLC,[80] Zhang *et al*., Adv. Funct. Mater. 33 (27), 2300805 (2023). Copyright 2023 Wiley-VCH GmbH,[8] Liao *et al*., Adv. Mater. 22 (47), 5393 (2010). Copyright 2010 Wiley-VCH GmbH.[72] Liao *et al*., Adv. Mater. Technol. 4 (2), 1800325 (2019). Copyright 2019 Wiley-VCH GmbH,[81] Voiculescu et al., Sens. Actuators A: Phys. 271, 356 (2018). Copyright 2018 Elsevier B.V.[82]

B. Fabrication of SCD MEMS

Due to its exceptional mechanical hardness and chemical stability, the microfabrication process for SCD cannot directly mirror the methods used for silicon and other wide bandgap semiconductors. The significant advancements in the growth and micromachining techniques of SCD have led to the development of specialized microfabrication approaches for SCD-based MEMS devices. These methods, include: (1) the smart-cut process utilizing ion-implantation-assisted lift-off (IAL) technology,[87,89,90] (2) diamond thinning via anisotropic plasma etching (APE),[88,91] and (3) diamond-on-insulator (DOI) technology, which involves bonding an SCD plate to an insulating substrate and thinning the plate to the designed level.[48,92]. The methods described above were thoroughly discussed in previous works.[37,40] Parikh et al. were the first to propose the Ion-Assisted Lift-Off (IAL) technique for fabricating freestanding diamond plates.[71] This process involves directly manufacturing devices on a thick SCD substrate. A key step in IAL is ion implantation, which creates an ion-damaged layer beneath the surface of the diamond, serving as a sacrificial layer during the subsequent etching process. Once this layer is selectively removed, the desired device structure is released. Based on the

microfabrication techniques for freestanding diamond plates, the IAL process has been further developed to create various SCD MEMS structures, which is also named smart-cut method.[37,72,74,87,89] This technique is particularly advantageous for producing SCD MEMS devices with an SCD-on-SCD configuration, offering precise control over dimensions from the nanoscale to the microscale and ensuring high reproducibility. The APE process begun with standard photolithography and etching on SCD material to define the design pattern, followed by anisotropic etching to release the device structure.[91] In contrast, the DOI technique involves bonding diamond to a foreign substrate and thinning it to the desired thickness through mechanical polishing and RIE/ICP etching. The device structure is then released by removing the oxide layer.[48,92,93] This method is advantageous for achieving high Q factors for diamond MEMS if the initial SCD plate has high crystal quality. Up to now, most of the SCD MEMS devices have been reported by the smart-cut method.

IV. SCD MEMS MAGNETIC SENSORS

The key components used in SCD MEMS devices are the mechanically vibrational resonators, which can detect various physical, chemical, and biological quantities through nano- and micro-scale displacements. In our previous research, we demonstrated that the Q factors of SCD cantilever resonators surpassed 10^6, which is one to two orders of magnitude higher than those of resonators made from silicon and other semiconductors.[7,94] SCD offers exceptional thermal stability due to its ultra-low thermal expansion and strong chemical resistance, making it an excellent platform for minimizing

interfacial diffusion. Given the excellent high-temperature properties of diamond, combining SCD MEMS with magnetostrictive thin films offers an effective approach to creating magnetic sensors that can operate from room temperature to high temperatures. Galfenol (FeGa), with its exceptionally high magnetostriction coefficient and a Curie temperature of around 950 K, presents as an ideal choice for high-temperature magnetic sensors.[5,95-97]. The combination of SCD and FeGa offers exceptional material properties, making their integration in MEMS devices a promising choice for creating high-performance and reliable magnetic sensors. Building on this concept, we developed MEMS magnetic sensors using FeGa thin films and SCD resonators. These sensors demonstrated both high sensitivity and reliability across a broad temperature range, from room temperature to extreme conditions.

A. Magnetrostrictive FeGa/SCD MEMS for magnetic sensors

The SCD MEMS resonators were fabricated using the smart-cut method, as detailed in our previous works.[31,32,37,98,99] The SCD MEMS magnetic sensors were constructed by integrating these resonators with a magnetostrictive FeGa thin film using RF magnetron sputtering. The resulting FeGa properties on SCD substate showed desirable soft magnetic properties, such as a low coercivity (*Hc*) of 26.2 Oe, a low saturation magnetization field (*Hs*) of 450 Oe, and a high remanence ratio (Mr/Ms) of 0.9.[100] To fabricate diamond based magnetic sensors with diverse structures, the interlayers of titanium (10 nm), tungsten carbide (20 nm), and a combination of titanium (5 nm) and tungsten carbide (10 nm) were deposited on the SCD substrates using RF magnetron

sputtering before the FeGa film growth. In SCD-based magnetic sensors, the Ti interlayer serves two primary functions: first, it reduced the possible reaction of between FeGa layer and the SCD, and second, it enhanced the interface adhesion, enabling efficient force transfer from the deformed FeGa film to the SCD cantilevers. The tungsten carbide (WC) interlayer helped align the FeGa film in the (200) crystal orientation, which has a higher magnetostrictive coefficient. Various multilayer structures of FeGa/SCD, FeGa/Ti/SCD, FeGa/WC/SCD, and FeGa/Ti/WC/SCD were fabricated for MEMS magnetic sensors which can work from room temperature (RT) to 773 K.

B. Magnetic sensing principle

The bending behavior of SCD beams can be solved exactly using the eigenmode approach. This analysis is based on the Euler–Bernoulli beam theory. Assuming the beam is made of a linear elastic material and experiences small deflections, $u(x, t)$, the motion of the beam follows the Euler–Bernoulli equation.[101,102]

$$EI\frac{\partial^4 u(x,\tau)}{\partial x^4} + \rho A\frac{\partial^2 u(x,\tau)}{\partial \tau^2} = 0 \quad (1)$$

The variable x represents position, while τ denotes time. The terms E and ρ correspond to the Young's modulus and the mass density of the beam, respectively. Similarly, A refers to the cross-sectional area of the beam, and I represents its moment of inertia. The solution to this differential equation consists of a combination of normal modes. These modes can be expressed as separate terms: one depending on position and the other on time, achieved through the method of separation of variables,

$$u(x,t) = \sum_{i=1}^{\infty} u_n(x)\cos(\omega t) \quad (2)$$

For a SCD MEMS resonator where the thickness and width are significantly smaller than the length, the vibrational behavior is primarily determined by flexural motion. The resonance frequency of the SCD MEMS resonator can be expressed as,

$$f_n == k\frac{t}{L^2}\sqrt{\frac{E}{\rho}} \tag{3}$$

where t and L are thickness and length of the SCD resonator, respectively. k is a parameter depending on the vibration mode and the resonator structure. For the first mode, k is equal to 0.162.

Fig. 5 presents the fundamental device structure and operating principle of a magnetic sensor that combines an SCD cantilever with a large magnetostrictive FeGa film. When an external magnetic field is applied to the cantilever, the stress state and Young's modulus of the bilayer system change, leading to a shift in the resonance frequency. The magnetic sensing mechanism of this SCD magnetic sensor relies on the ΔE effect, which refers to changes in the Young's modulus under magnetic fields.[15,103] This effect arises from the deformation or dimension changes in the soft magnetic material due to the applied magnetic field. A higher magnetostrictive constant in the soft magnetic material amplifies the ΔE effect. Upon applying an external magnetic field without changing other quantalities, the resonance frequency shift of the SCD-based magnetic sensor can be expressed as,

$$\Delta f_T = |f_{TH} - f_{T0}| = 0.162\frac{t}{L^2\sqrt{\rho}}\left|\sqrt{E_{TH}} - \sqrt{E_{T0}}\right| \tag{3}$$

where E_H, and E_0 are the Young's modulus with and without applying the magnetic field, respectively. f_{TH} and f_{T0} represent the resonance frequencies of the magnetic sensor with and without applying the magnetic field at a certain temperature. The magnetic sensitivity

of the FeGa/SCD MEMS sensor is characterized by the frequency sensitivity, D*f*/D*H*, where D*H* is the variation of the magnetic field.

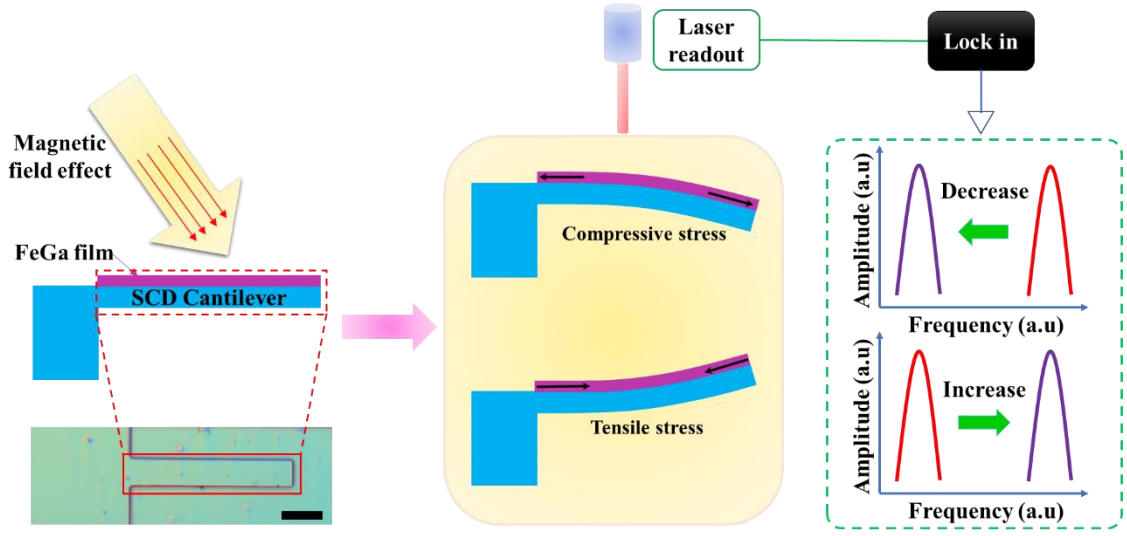

FIG. 5. Schematic diagram of sensing principle of a SCD resonant magnetic sensor that employs a FeGa/SCD cantilever resonator with a heterogeneous structure. When a magnetic field is applied, the magnetostrictive effect alters the Young's modulus and stress condition of the cantilever. These changes in stress affect the resonance frequency of the sensor, with compressive stress causing a decrease in resonance frequency and tensile stress causing an increase. The cantilever's vibrations are measured using optical readout in conjunction with a lock-in amplifier. Scale bar: 20 μm. Reprinted with permission from Zhang *et al*., Carbon, 152, 788-795 (2019). Copyright 2021 Elsevier B.V.[37]

V. SCD MEMS for HIGH TEMPERATURE MAGNETIC SENSING

A. Thermal-stability of SCD MEMS

The temperature coefficient of resonance frequency (TCF), defined as TCF = ($\partial f/f_0 \partial$T), was utilized to assess the thermal stability of SCD cantilevers. f_0 represents the fundamental resonance frequency at 300 K. According to this equation, the resonance frequency is strongly influenced by the Young's modulus of the cantilever. Additionally, temperature has an inverse effect on the Young's modulus of the material.[104-106]

$$E = E_{T0} - ATexp(-\frac{T_0}{T}) \quad (4)$$

E_{T0} represents the Young's modulus of the material at temperature of T_0. A is a constant.

The resonance frequency of the cantilever decreases as temperature increased, due to the reduction in Young's modulus (**Figs. 6(a) and (b)**). **Fig. 6(c)** illustrates that the TCF of the bare SCD cantilever was below -3.2 ppm/K over a temperature range from 300 K to 773 K. This TCF is notably lower than that of Si, which is about -35 ppm/K.[107,108] It reveals that the SCD cantilever can offer a promising platform for MEMS devices capable of stably working under high temperatures. Furthermore, the Q factors of the SCD cantilevers remained above 3000 at 773 K (**Fig. 6(d)**). The Q factor exhibited a negative temperature dependence. As temperature increased, the energy dissipation also increased.

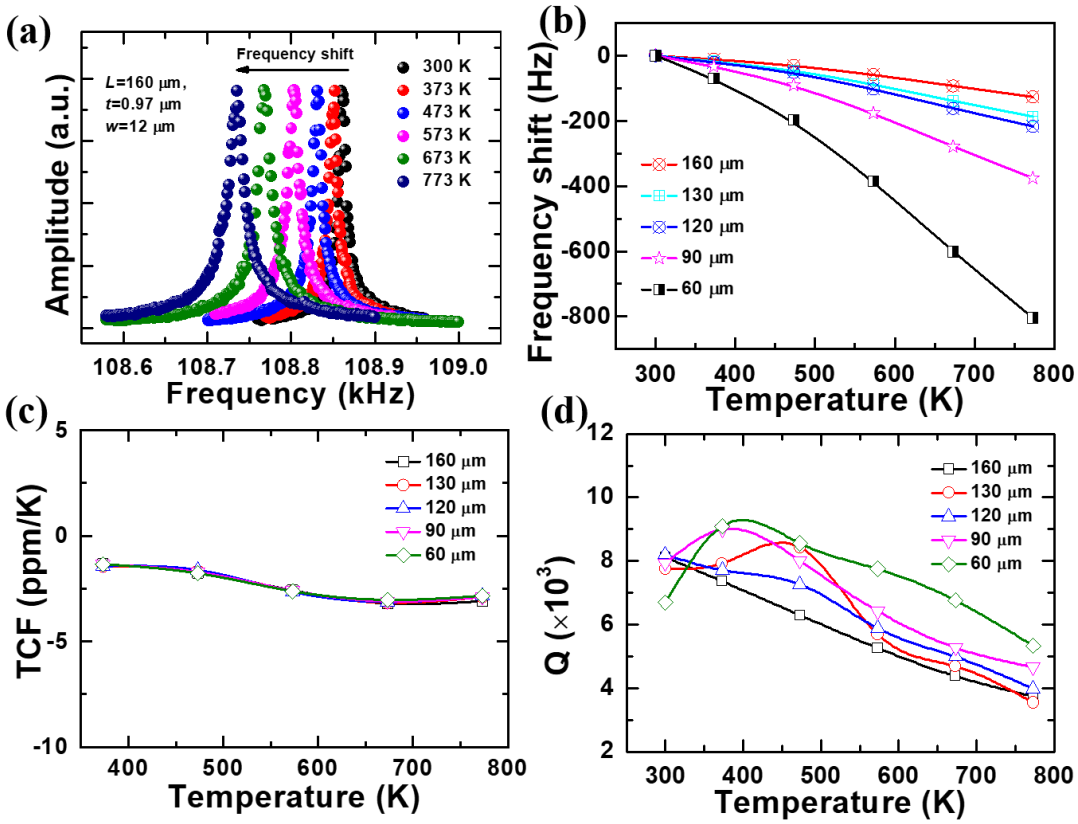

FIG. 6. (a) Resonance frequency shifts of a bare SCD cantilever with changing measurement temperature. (b) Temperature-dependent changes in resonance frequency shifts of bare SCD cantilevers of different lengths. (c) Temperature coefficients of the resonance frequencies for SCD cantilevers. (d) Temperature-dependent variations in the Q factors of SCD cantilevers. Reprinted with permission from Zhang *et al*., Mater. Res. Lett., 8(5), 180-186 (2020) Copyright 2020 Informa UK Limited.[31]

B. High-temperature SCD MEMS magnetic sensing

The integration of a magneto-strictive FeGa thin film with a SCD cantilever offers a promising method for developing microscale magnetic sensors based on the ΔE effect from room temperature to high temperatures.[15-17,109]. **Fig. 7(a)** schematically shows a magnetic sensor composed of a 80 nm-thick FeGa film deposited on a SCD cantilever, which is utilized to fabricate MEMS magnetic sensor at room temperature.[37] The frequency response of the FeGa/SCD sensor with a length of 160 μm to the magnetic field is shown in **Fig. 7(b)**. As the magnetic field increased, the resonance frequency of the sensor decreased. The changes in resonance frequency of the FeGa/SCD sensor exhibited a linear relationship with the applied magnetic field, regardless of the length of the cantilevers (Fig. 7(c)). The magnetic field sensitivity was around 4.83 Hz/mT for the FeGa/SCD sensor with a length of 60 μm. Additionally, the variations in magnetostrictive force of the FeGa/SCD cantilevers subjected to different magnetic field strengths was calculated to be around 10 fN (**Fig. 7(d)**).[37] Presently, the magnetic sensors that rely on resonance frequency shifts in response to magnetic fields are commonly based on the Lorentz force and magnetostrictive force. **Table 1** summarizes the magnetic sensitivities of various MEMS magnetic sensors at room temperature, showing that the magnetostrictive force MEMS sensors have higher sensitivity than those of Lorentz-type. The sensitivity of the FeGa/SCD sensor was significantly improved by incorporating a Ti thin film.

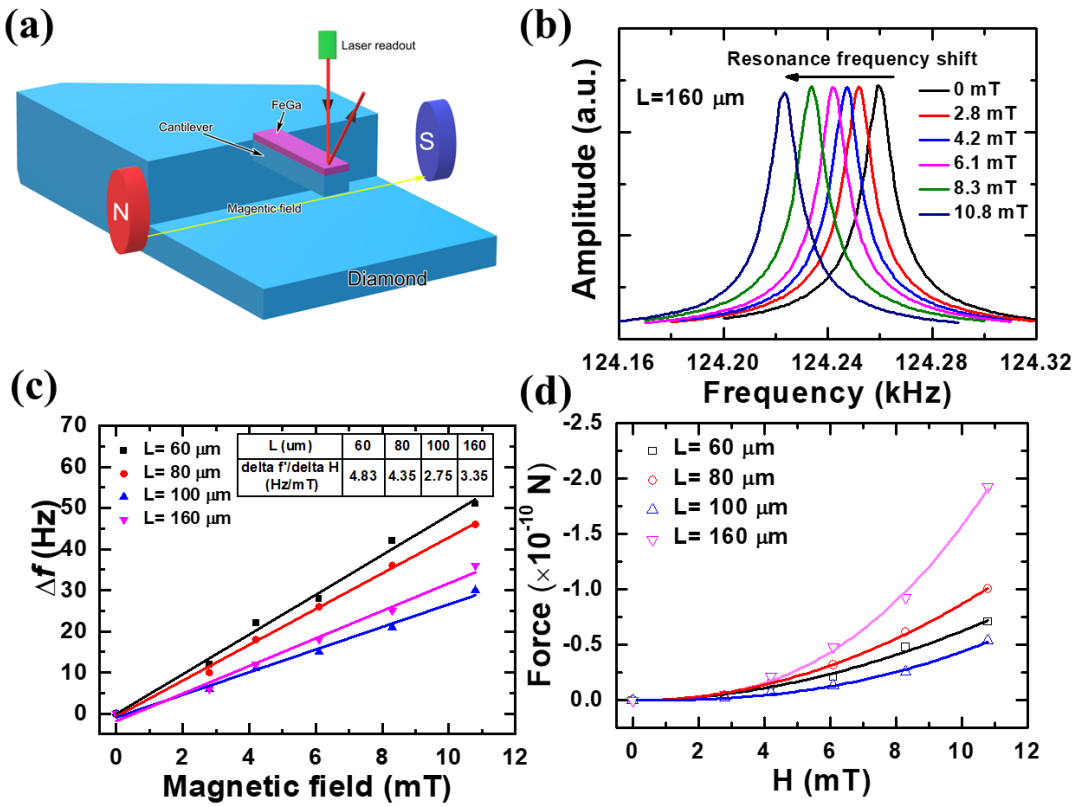

FIG. 7. (a) A schematic diagram of a magnetic sensor utilizing a FeGa/SCD sensor. (b) The resonance frequency response of a 160 μm-length FeGa/SCD sensor as the applied magnetic fields vary. (c) The relationship between the resonance frequency shifts and (d) the detectable force of the FeGa/SCD sensors in response to magnetic fields. A negative force indicates compressive stress. Reprinted with permission from Zhang *et al*., Carbon, 152, 788-795 (2019). Copyright 2019 Elsevier B.V.[37]

TABLE 1 An evaluation of the magnetic sensitivities of different MEMS magnetic sensors at room temperature.

Magnetic sensor	Material	f (◊10^3)	Q	Sensitivity (Hz/mT)	Ref.
Lorentz force	Si	38.074	15000	0.09	110
Lorentz force	Si	175	~600	60.00	10
Lorentz force	SOI	49.3	100000	0.01	111
Lorentz force	SOI	22.6	540	0.59	112
Magnetostrictive force	FeGa/quartz	38.199	3318	35.00	5
Magnetostrictive force	FeGa/PZT	12.450	1132	5.47	113
Magnetostrictive force	FeGa/SCD	949.966	8201	4.83	37

Magnetostrictive force	FeGa/Ti/SCD	147.916	3889	35.6	[32]

Silicon-on-insulator (SOI), lead zirconate titanate (PZT)

High-temperature magnetic sensors utilizing the FeGa/SCD MEMS resonators were developed up to 573 K [31]. The frequency shifts at elevated temperatures increased linearly with the applied magnetic field. Notably, the FeGa/SCD cantilever maintained a stable response to the magnetic field even at 573 K. The intrinsic magnetic noise (b_n) of the magnetic sensor, governed by thermomechanical noise, is represented by the following expression,[114]

$$b_n = \frac{\mu_0}{2}\left(\frac{dH}{df}\right)\sqrt{\frac{2\pi k_B T f_0}{QV\sigma}} \quad (5)$$

The magnetic sensitivity is represented by $m_0(dH/df)$, while s denotes stress. To enhance both the operating temperature and magnetic sensitivity, a Ti layer was introduced between the FeGa and SCD, as the FeGa/Ti/SCD resonator structure.[32]. The change in resonance frequency of a 100 μm-long FeGa/Ti/SCD cantilever when subjected to magnetic fields at different temperatures during heating process is displayed in **Fig. 8(a)**. The frequency shifts showcased a linear dependence on magnetic field, reaching a maximum sensitivity of 71.1 Hz/mT at temperatures up to 773 K (**Fig. 8(b)**).

The magnetic noise levels of the FeGa/Ti/SCD resonator sensor at 300 K and 773 K were examined through the relationship between the frequency shifts and the magnetic fields. **Figs. 8(c) and (d)** present the magnetic noise spectra for the 100 μm-long FeGa/Ti/SCD resonator, showing low magnetic noise levels of ~ 20 nT/ √ Hz at 300 K

and ~10 nT/ √ Hz at 773 K, respectively. Using Eq. (5), the intrinsic magnetic noise of the FeGa/Ti/SCD magnetic sensor was estimated to be approximately 206.7 pT/ √ Hz at 300 K and 212.4 pT/ √ Hz at 773 K, respectively. The observed discrepancy between the measured and estimated noise levels may be due to the noise characteristics of the measurement apparatus. The improved thermal stability of the SCD MEMS magnetic sensor is attributed to the enhanced adhesion between the FeGa and SCD facilitated by the Ti layer. Additionally, **Table 2** compares the magnetic sensing performance of the FeGa/Ti/SCD sensor with other high-temperature magnetic sensors. The comparison reveals that the SCD-based sensor offers lower noise, and higher thermal reliability compared to its counterparts.

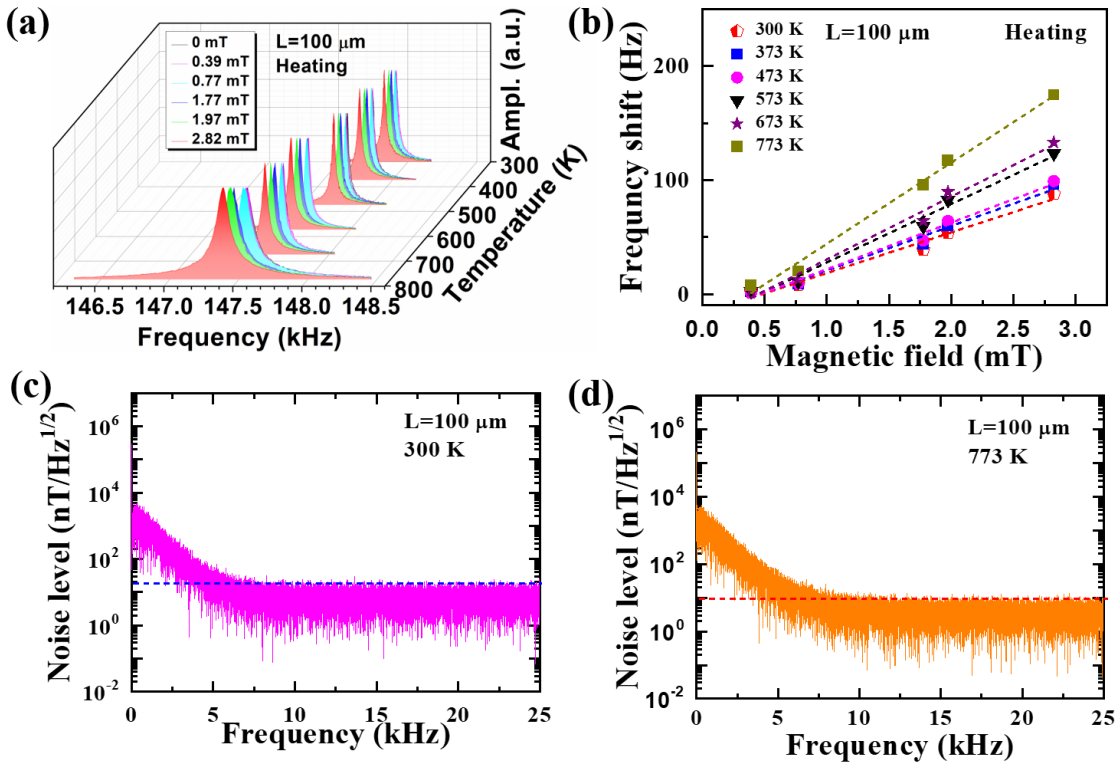

FIG. 8.1 (a) Resonance spectra of a FeGa/Ti/SCD sensor with changing the measurement temperatures and the external magnetic fields. (b) Dependences of resonance frequency shifts on magnetic fields during the heating process. (c) and (d) Magnetic noise spectra

of the FeGa/Ti/SCD sensor at temperatures of 300 K and 773 K, respectively [32]. Reprinted with permission from Zhang *et al*., ACS Appl. Mater. Interfaces, 12(20), 23155-23164 (2020). Copyright 2020, American Chemical Society.

TABLE 2 Comparison of high-temperature performances of various magnetic sensors [32]. Reprinted with permission from Copyright 2020, American Chemical Society

Magnetic sensor	Materials	Sensitivity	Noise level	Working temperature	Ref.
AMR	Si-based	--	~2.6 nT/√Hz	498 K	[115]
Hall	Si	--	>82 nT/√Hz	673 K	[116]
Hall	AlGaN/GaN	--	35 μT/√Hz	873 K	[117]
Hall	4H-SiC	80 V/(A·T)	--	770 K	[118]
Fluxgate	Cu coil	--	0.79 nT/√Hz	523 K	[119]
MEMS	FeGa/Ti/SCD	71.1 Hz/mT	10 nT/√Hz	773 K	[32]

C. On-chip SCD MEMS magnetic sensors

For highly integrated MEMS magnetic sensors, an electrical system that combines actuation, sensing, and signal readout is desirable. An on-chip SCD MEMS magnetic sensor designed for high-temperature applications was proposed and demonstrated, utilizing a multifunctional magnetostrictive FeGa film for harmonic actuation, magnetic sensing, and resonance signal readout.[8] The Au/FeGa/Ti was deposited on the SCD substrate as the gate (called G) electrode for the on-chip actuation and on the SCD cantilevers as source-drain (called S-D) electrodes to sense the magnetic fields and electrically readout the resonance signal (**Fig. 9(a)**). A preliminary SCD-based magnetic transducer array comprising four cantilevers integrated on the same chip for magnetic transducing with all-electrical actuation and sensing were fabricated (**Fig. 9(b)**). The

resonance frequency spectra shift of the 160 μm-long SCD-based magnetic sensor caused by applying a magnetic field of 2.82 mT with the temperature increasing from RT to 773 K, as shown in **Fig. 9(c)**. The SCD-based magnetic transducer *via* the on-chip actuation and sensing had a stable magnetic sensitivity of 3.2 Hz/ mT at various temperatures. Due to the independent resonance vibrations of each magnetic sensor, we successfully achieved parallel signal readout from the four transducers. The resonance frequency spectra of the transducer array displayed four distinct peaks with and without the presence of a 0.28 mT magnetic field **(Fig. 9(d))**. This study opens the avenue for the integration of SCD-based MEMS magnetic transducers with electronics.

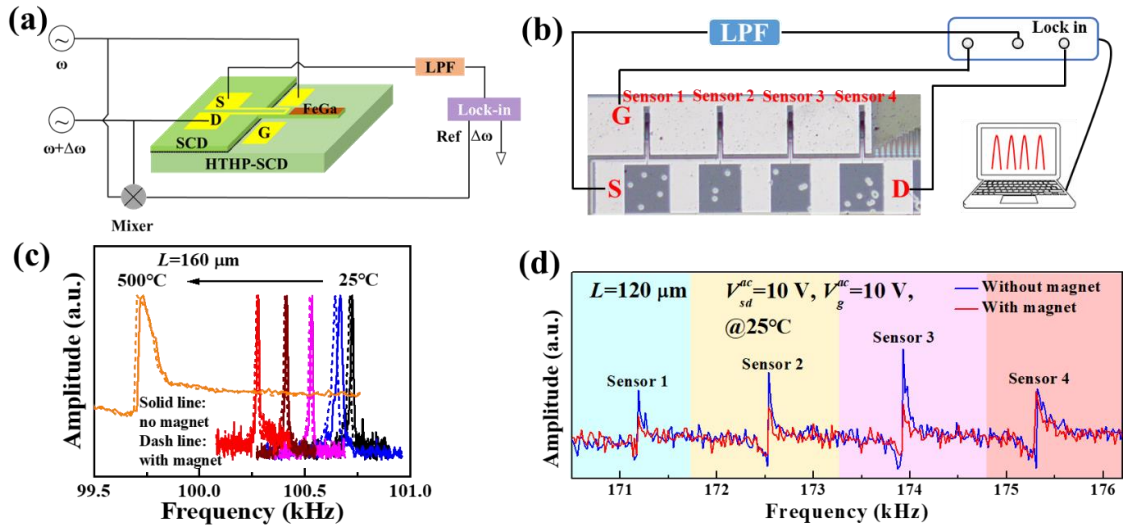

FIG. 9. On-chip SCD MEMS magnetic transducer. **a** Schematic diagram of the measurement setup for the SCD-based cantilever magnetic transducer with the on-chip self-sensing and actuation configuration. LPF: low frequency filter. V_g^{ac} was applied to the G electrode. And V_{sd}^{ac} was connected to the S–D electrodes. **b** Optical image of an SCD-based magnetic transducer array. **c** Resonance frequency shift of a 160 μm-long SCD-based cantilever transducer as a function of the measurement temperature at a magnetic field of 2.82 mT, and at V_{sd}^{ac} =4 V and V_g^{ac}=7 V from RT to 773K. The peak amplitude of etch spectrum was normalized. **d** Resonance frequency shifts of the magnetic transducer array under a 2.82 mT magnetic field at V_{sd}^{ac} = 10 V and V_g^{ac} = 10 V @300K. Reprinted with permission from Zhang *et al.*, Adv. Funct. Mater. 33 (27), 2300805 (2023). Copyright 2024 Wiley-VCH GmbH.[8]

VI. CURRENT CHALLENGES and PERSPECTIVES

For the development of the highly-reliable diamond-based MEMS magnetic sensors at high temperatures, the following challenges need be considered. 1) Thermal Stability: diamond MEMS magnetic sensors are renowned for their exceptional thermal stability. However, ultrahigh temperatures (>773 K) can still pose challenges for the heterostructures. Prolonged exposure to extreme temperatures can lead to degradation of the interface between diamond and the functional magnetic thin films due to lattice and thermal expansion coefficient discrepancy. The interface engineering between diamond and the magnetic material requires further optimization. 2) Sensitivity limitation: high temperatures introduce additional thermal noise, affecting the sensitivity and accuracy of the diamond magnetic sensors. Balancing sensitivity with thermal noise mitigation is crucial. 3) Integration with electronics: integrating electronic components that can withstand high temperatures remains a significant challenge. Conventional electronic materials and electronics may fail under extreme thermal conditions, requiring the development of high-temperature-compatible electronics and multi-technology solutions. 4) Calibration and measurement accuracy. High temperatures cause thermal drift in the calibration of diamond-based sensors, impacting their measurement precision. Ensuring accurate sensor performance demands advanced calibration methods and effective temperature compensation algorithms.

For realizing high-sensitivity and high-reliability SCD magnetic sensors, the

following research topics can be conducted: 1) Advanced materials development: research need focusing on optimizing the current or developing novel diamond heterostructures with the magnetic materials that enhance thermal resistance and minimize degradation. Such as the Tb-doped FeGa fim for improving the durability and performance of diamond MEMS sensors at high temperatures. 2) Sensitivity improved technologies. In order to realize high sensitivity of diamond-based magnetic sensors, diamond resonators in nanoscale (the thickness < 100 nm) can be fabricated. The enhancement of the Q factor is crucial for increasing the signal-to-noise ratio and minimizing magnetic noise. Based on the high sensitivity for the nanoscale diamond resonator, the dependence of the resonance frequency and Q factor on magnetic noise level is evaluated in **Fig. 10**. A low magnetic noise level of 383.3 $fT/Hz^{1/2}$ is expected to achieve assuming the diamond cantilever thickness is reduced to 100 nm and the length to 1 μm and the Q factor of one million still maintains. A refined method for improving the Q factor in diamond resonators may be adopted, like the utilizing the established dissipation dilution mechanism.[33,34] 3) Hetero-integration with other technologies. Combining diamond MEMS sensors with other sensing technologies or data processing systems is essential for practical applications. Multimodal sensing and data fusion techniques may enhance the overall performance and reliability of these sensors. 4) Calibration Techniques. Future work should involve the development of advanced calibration methods and real-time temperature compensation algorithms for diamond magnetic sensors under high temperatures. These approaches will help maintain accuracy and precision under varying thermal conditions. By exploiting diamond sensors array, MEMS magnetic imaging sensor can be also devleoped.[8]

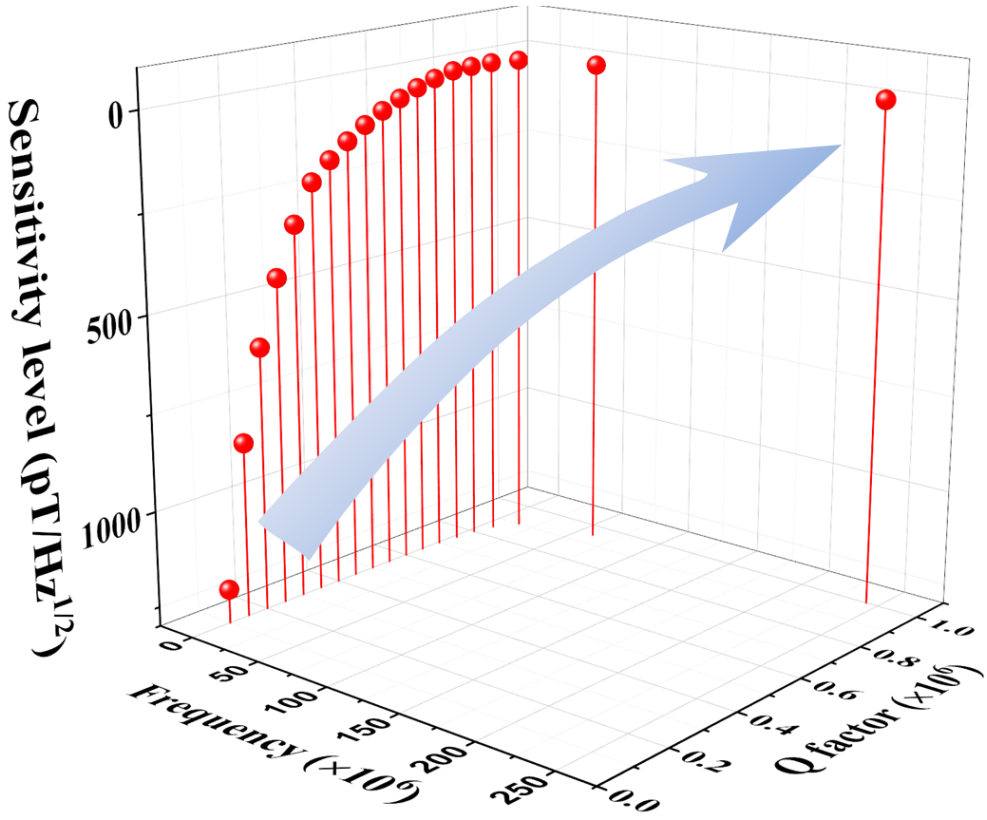

FIG. 10. Perspective on the magnetic sensitivity of diamond MEMS magnetic sensors.

V. CONCLUSION

Diamond MEMS technology holds immense potential for revolutionizing magnetic sensor applications in extreme environments. By leveraging the classical theory of the magnetostrictive effect, diamond MEMS resonators combined with highly thermally stable soft magnetic materials present a promising approach to develop sensors capable of withstanding high temperatures. This perspective provides an overview of diamond MEMS magnetic sensors designed for such conditions, covering fundamental material properties, fabrication methods, and the progression of these structures into magnetic sensors, from room temperature to high-temperature magnetic sensing applications. Despite renewed interest in this field, spurred by advancements in diamond MEMS, challenges remain. These include enhancing magnetic sensitivity, overcoming operational

temperature limitations, and developing suitable integration and calibration technologies to meet real-application standards. With ongoing research, the creation of diamond MEMS arrays and their integration with electronics in advanced systems shows potential for groundbreaking advancements in magnetic field imaging at extreme temperatures and beyond.

Author Declarations

Conflict of Interest

The authors have no conflicts to disclose.

Author Contributions

Zilong Zhang: Data curation (equal); Formal analysis (equal); Investigation (equal); Methodology (equal); Validation (equal); Writing–original draft (equal); Writing–review & editing (equal).

Keyun Gu: Writing –review & editing (equal).

Masaya Toda: Writing –review & editing (equal).

Meiyong Liao: Conceptualization (equal); Data curation (equal); Formal analysis (equal); Funding acquisition; (equal); Methodology (equal); Project; Writing–original draft (equal); Writing –review & editing (equal).

Acknowledgements

This was partially supported by a Grant-in-Aid of JSPS KAKENHI (Grant Number 24H00287, 22K18957, and 24K00828), Bilateral joint research between JSPS/CAS, and Advanced Research Infrastructure for Materials and Nanotechnology in Japan (ARIM JPMXP1223NM5297) of the Ministry of Education, Culture, Sports, and Technology (MEXT) of Japan.

References

[1] J. Lenz and S. Edelstein, IEEE Sen. J. **6** (3), 631 (2006).

[2] A. Herrera-May, L. Aguilera-Cortés, P. García-Ramírez, and E. Manjarrez, Sensors **9** (10), 7785 (2009).

[3] Y. Wang, J. Li, and D. Viehland, Mater. Today **17** (6), 269 (2014).

[4] X. Zhao, Y. Bai, Q. Deng, C. Ai, X. Yang, and D. Wen, IEEE Sen. J. **17** (18), 5849 (2017).

[5] L. Bian, Y. Wen, Y. Wu, P. Li, Z. Wu, Y. Jia, and Z. Zhu, IEEE Trans. Electron Devices **65** (6), 2585 (2018).

[6] D. Robbes, Sens. Actuators A: Phys. **129** (1-2), 86 (2006).

[7] H. Wu, L. Sang, Y. Li, T. Teraji, T. Li, M. Imura, J. You, Y. Koide, M. Toda, and M. Liao, Phys. Rev. Mater. **2** (9), 090601 (2018).

[8] Z. Zhang, W. Zhao, G. Chen, M. Toda, S. Koizumi, Y. Koide, and M. Liao, Adv. Funct. Mater. **33** (27), 2300805 (2023).

[9] A. Herrera-May, P. García-Ramírez, L. Aguilera-Cortés, J. Martínez-Castillo, A. Sauceda-Carvajal, L. García-González, and E. Figueras-Costa, J. Micromech. Microeng. **19** (1), 015016 (2008).

[10] R. Sunier, T. Vancura, Y. Li, K.-U. Kirstein, H. Baltes, and O. Brand, J. Microelectromech. Syst. **15** (5), 1098 (2006).

[11] D. Wickenden, J. Champion, R. Osiander, R. Givens, J. Lamb, J. Miragliotta, D. Oursler, and T. Kistenmacher, Acta Astronaut. **52** (2-6), 421 (2003).

[12] A. Herrera-May, L. Aguilera-Cortés, L. García-González, and E. Figueras-Costa, Microsystem technologies **15** (2), 259 (2009).

[13] Z. Kádár, A. Bossche, P. Sarro, and J. Mollinger, Sens. Actuat. A: Phys. **70** (3), 225 (1998).

[14] H. Emmerich and M. Schofthaler, IEEE Trans. Electron Dev. **47** (5), 972 (2000).

[15] B. Gojdka, R. Jahns, K. Meurisch, H. Greve, R. Adelung, E. Quandt, R. Knöchel, and F. Faupel, Appl. Phys. Lett. **99** (22), 223502 (2011).

[16] R. Jahns, S. Zabel, S. Marauska, B. Gojdka, B. Wagner, R. Knöchel, R. Adelung, and F. Faupel, Appl. Phys. Lett. **105** (5), 052414 (2014).

[17] S. Zabel, C. Kirchhof, E. Yarar, D. Meyners, E. Quandt, and F. Faupel, Appl. Phys. Lett. **107** (15), 152402 (2015).

[18] S. Zabel, J. Reermann, S. Fichtner, C. Kirchhof, E. Quandt, B. Wagner, G. Schmidt, and F. Faupel, Appl. Phys. Lett. **108** (22), 222401 (2016).

[19] N. Okada, T. Sasabuchi, K. Koike, and T. Mineta, Electr. Commun. Jpn. **101** (3), 90 (2018).

[20] T. Nan, Y. Hui, M. Rinaldi, and N. X. Sun, Sci. Rep. **3** (1), 1 (2013).

[21] H. Greve, E. Woltermann, H.-J. Quenzer, B. Wagner, and E. Quandt, Appl. Phys. Lett. **96** (18), 182501 (2010).

[22] S. Marauska, R. Jahns, H. Greve, E. Quandt, R. Knöchel, and B. Wagner, J. Micromech. Microeng. **22** (6), 065024 (2012).

[23] R. Jahns, H. Greve, E. Woltermann, E. Quandt, and R. H. Knochel, IEEE Trans. Instrum. Meas. **60** (8), 2995 (2011).

[24] Z. Zhao, M. Toda, and T. Ono, Appl. Phys. Lett. **124** (25) (2024).
[25] M. Cheng, Z. Hu, J. Wu, C. Wang, Y. Du, D. Xian, Q. Mao, B. Tian, M. Guan, and Z. Wang, IEEE Trans. Magn. **58** (1), 1 (2021).
[26] T. Ono and M. Esashi, Rev. Sci. Instrum. **74** (12), 5141 (2003).
[27] B. Spetzler, E. V. Golubeva, C. Müller, J. McCord, and F. Faupel, Sensors **19** (21), 4769 (2019).
[28] B. Spetzler, C. Kirchhof, E. Quandt, J. McCord, and F. Faupel, Phys. Rev. Appl. **12** (6), 064036 (2019).
[29] M. Li, A. Matyushov, C. Dong, H. Chen, H. Lin, T. Nan, Z. Qian, M. Rinaldi, Y. Lin, and N. X. Sun, Appl. Phys. Lett. **110** (14), 143510 (2017).
[30] A. Kittmann, P. Durdaut, S. Zabel, J. Reermann, J. Schmalz, B. Spetzler, D. Meyners, N. X. Sun, J. McCord, and M. Gerken, Sci. Rep. **8** (1), 1 (2018).
[31] Z. Zhang, Y. Wu, L. Sang, H. Wu, J. Huang, L. Wang, Y. Takahashi, R. Li, S. Koizumi, and M. Toda, Mater. Res. Lett. **8** (5), 180 (2020).
[32] Z. Zhang, H. Wu, L. Sang, Y. Takahashi, J. Huang, L. Wang, M. Toda, I. M. Akita, Y. Koide, and S. Koizumi, ACS Appl. Mater. Interfaces **12** (20), 23155 (2020).
[33] H. Sun, Z. Zhang, Y. Liu, G. Chen, T. Li, and M. Liao, Adv. Quantum Technol. **6** (11), 2300189 (2023).
[34] G. Chen, S. Koizumi, Y. Koide, and M. Liao, Accounts Mater. Res. (2024).
[35] A. Uranga, J. Verd, and N. Barniol, Microelectron. Eng. **132**, 58 (2015).
[36] Y. Tao, J. M. Boss, B. Moores, and C. L. Degen, Nat. Commun. **5** (1), 3638 (2014).
[37] Z. Zhang, H. Wu, L. Sang, J. Huang, Y. Takahashi, L. Wang, M. Imura, S. Koizumi, Y. Koide, and M. Liao, Carbon **152**, 788 (2019).
[38] R. Lifshitz and M. L. Roukes, Phys. Rev. B **61** (8), 5600 (2000).
[39] M. Liao and Y. Koide, Crit. Rev. Solid State Mater. Sci. **36** (2), 66 (2011).
[40] M. Liao, Functional Diamond **1** (1), 29 (2022).
[41] A. M. Zaitsev, *Optical properties of diamond: a data handbook*. (Springer Science & Business Media, 2013).
[42] W. Gajewski, P. Achatz, O. A. Williams, K. Haenen, E. Bustarret, M. Stutzmann, and J. A. Garrido, Phys. Rev. B **79** (4), 045206 (2009).
[43] M. Akaishi and S. Yamaoka, Mater. Sci. Eng. A **209** (1-2), 54 (1996).
[44] C.-H. Su, AIP Adv. **5** (5), 057118 (2015).
[45] M. Liao, Y. Koide, and L. Sang, Novel Aspects of Diamond: From Growth to Applications, 91 (2019).
[46] H. Yang, Y. Ma, and Y. Dai, Functional Diamond **1** (1), 150 (2022).
[47] C. E. Nebel, Functional Diamond **3** (1), 2201592 (2023).
[48] P. Ovartchaiyapong, L. Pascal, B. Myers, P. Lauria, and A. Bleszynski Jayich, Appl. Phys. Lett. **101** (16), 163505 (2012).
[49] N. Sepulveda, D. Aslam, and J. P. Sullivan, Phys. Rev. B **15** (2-3), 398 (2006).
[50] L. Sekaric, J. Parpia, H. G. Craighead, T. Feygelson, B. Houston, and J. Butler, Appl. Phys. Lett. **81** (23), 4455 (2002).
[51] A. Hutchinson, P. Truitt, K. Schwab, L. Sekaric, J. Parpia, H. G. Craighead, and J. Butler, Appl. Phys. Lett. **84** (6), 972 (2004).
[52] A. Gaidarzhy, M. Imboden, P. Mohanty, J. Rankin, and B. W. Sheldon, Appl. Phys. Lett. **91** (20) (2007).
[53] V. P. Adiga, A. Sumant, S. Suresh, C. Gudeman, O. Auciello, J. Carlisle, and R. W. Carpick, Phys. Rev. B **79** (24), 245403 (2009).

[54] M. Poggio, M. Jura, C. Degen, M. Topinka, H. Mamin, D. Goldhaber-Gordon, and D. Rugar, Nat. Phys. **4** (8), 635 (2008).
[55] D. Saya, K. Fukushima, H. Toshiyoshi, G. Hashiguchi, H. Fujita, and H. Kawakatsu, Sen. Actuat. A: Phys. **95** (2-3), 281 (2002).
[56] Q. Yu, G. Qin, C. Darne, C. Cai, W. Wosik, and S.-S. Pei, Sen. Actuat. A Phys. **126** (2), 369 (2006).
[57] X. Li, T. Ono, Y. Wang, and M. Esashi, presented at the Technical Digest. MEMS 2002 IEEE International Conference. Fifteenth IEEE International Conference on Micro Electro Mechanical Systems (Cat. No. 02CH37266), 2002.
[58] D.-W. Lee, J.-H. Kang, U. Gysin, S. Rast, E. Meyer, M. Despont, and C. Gerber, J. Micromech. Microeng. **15** (11), 2179 (2005).
[59] J. Lu, T. Ikehara, Y. Zhang, T. Mihara, T. Itoh, and R. Maeda, presented at the 2008 Symposium on Design, Test, Integration and Packaging of MEMS/MOEMS, 2008.
[60] K. Adachi, N. Watanabe, H. Okamoto, H. Yamaguchi, T. Kimoto, and J. Suda, Sen. Actuat. A Phys. **197**, 122 (2013).
[61] R. Boubekri, E. Cambril, L. Couraud, L. Bernardi, A. Madouri, M. Portail, T. Chassagne, C. Moisson, M. Zielinski, and S. Jiao, J. Appl. Phys. **116** (5) (2014).
[62] P. Guzman, T. Dinh, A. Qamar, J. Lee, X. Zheng, P. Feng, M. Rais-Zadeh, H.-P. Phan, T. Nguyen, and A. R. M. Foisal, Sen. Actuat. A Phys. **343**, 113678 (2022).
[63] S. Wang, L. C. Popa, and D. Weinstein, presented at the Proc. Solid-State Sens., Actuators, Microsyst. Workshop (Hilton Head), 2014.
[64] J. Montague, K. Bertness, N. Sanford, V. Bright, and C. Rogers, Appl. Phys. Lett. **101** (17) (2012).
[65] V. Gokhale, J. Roberts, and M. Rais-Zadeh, presented at the 2011 16th International Solid-State Sensors, Actuators and Microsystems Conference, 2011.
[66] L. Sang, H. Sun, X. Yang, T. Li, B. Shen, and M. Liao, presented at the 2020 IEEE International Electron Devices Meeting (IEDM), 2020.
[67] A. K. Mallik, R. Rouzbahani, F. Lloret, R. Mary Joy, and K. Haenen, Functional Diamond **3** (1), 2295346 (2023).
[68] K. Ekinci and M. Roukes, Rev. Sci. Instrum. **76** (6), 061101 (2005).
[69] A. D. Greentree, B. A. Fairchild, F. M. Hossain, and S. Prawer, Mater. Today **11** (9), 22 (2008).
[70] I. Aharonovich, A. D. Greentree, and S. Prawer, Nat. Photonics **5** (7), 397 (2011).
[71] N. Parikh, J. Hunn, E. McGucken, M. Swanson, C. White, R. Rudder, D. Malta, J. Posthill, and R. Markunas, Appl. Phys. Lett. **61** (26), 3124 (1992).
[72] M. Liao, S. Hishita, E. Watanabe, S. Koizumi, and Y. Koide, Adv. Mater. **22** (47), 5393 (2010).
[73] Z. Zhang, K. Gu, G. Chen, L. Sang, T. Teraji, Y. Koide, S. Koizumi, M. Toda, and M. Liao, Adv. Mater. Technol., 2400153 (2024).
[74] J. Fu, T. Zhu, Y. Liang, Z. Liu, R. Wang, X. Zhang, and H.-X. Wang, Sci. Rep. **9** (1), 1 (2019).
[75] A. N. Obraztsov, P. G. Kopylov, B. A. Loginov, M. A. Dolganov, R. R. Ismagilov, and N. V. Savenko, Rev. Sci. Instrum. **81** (1), 13703.
[76] F. T. Tuyakova, E. A. Obraztsova, and R. R. Ismagilov, J. Nanophotonics **10** (1), 012517 (2015).
[77] Y. Tao and C. L. Degen, Nano Lett. **15** (12), 7893 (2015).
[78] M. Liao, H. Sun, and S. Koizumi, Adv. Sci. **11** (13), 2306013 (2024).
[79] P. Maletinsky, S. Hong, M. S. Grinolds, B. Hausmann, M. D. Lukin, R. L. Walsworth, M. Loncar, and

A. Yacoby, Nat. Nanotechnol. **7** (5), 320 (2012).
[80] P. Appel, E. Neu, M. Ganzhorn, A. Barfuss, M. Batzer, M. Gratz, A. Tschöpe, and P. Maletinsky, Rev. Sci. Instrum. **87** (6), 063703 (2016).
[81] M. Liao, L. Sang, T. Teraji, S. Koizumi, and Y. Koide, Adv. Mater. Technol. **4** (2), 1800325 (2019).
[82] I. Voiculescu, M. Liao, M. Zakerin, R. Berger, T. Ono, and M. Toda, Sen. Actuat. A Phys. **271**, 356 (2018).
[83] M. K. Bhaskar, D. D. Sukachev, A. Sipahigil, R. E. Evans, M. J. Burek, C. T. Nguyen, L. J. Rogers, P. Siyushev, M. H. Metsch, and H. Park, Phys. Rev. Lett. **118** (22), 223603 (2017).
[84] M. J. Burek, Y. Chu, M. S. Liddy, P. Patel, J. Rochman, S. Meesala, W. Hong, Q. Quan, M. D. Lukin, and M. Lončar, Nat. Commun. **5** (1), 1 (2014).
[85] M. Mitchell, B. Khanaliloo, D. P. Lake, T. Masuda, J. P. Hadden, and P. E. Barclay, Optica **3** (9), 963 (2016).
[86] M. Aspelmeyer, T. J. Kippenberg, and F. Marquardt, Rev. Modern Phys. **86** (4), 1391 (2014).
[87] P. Olivero, S. Rubanov, P. Reichart, B. C. Gibson, S. T. Huntington, J. Rabeau, A. D. Greentree, J. Salzman, D. Moore, and D. N. Jamieson, Adv. Mater. **17** (20), 2427 (2005).
[88] M. J. Burek, N. P. De Leon, B. J. Shields, B. J. Hausmann, Y. Chu, Q. Quan, A. S. Zibrov, H. Park, M. D. Lukin, and M. Lončar, Nano Lett. **12** (12), 6084 (2012).
[89] M. Liao, C. Li, S. Hishita, and Y. Koide, J. Micromech. Microeng. **20** (8), 085002 (2010).
[90] M. Liao, M. Toda, L. Sang, T. Teraji, M. Imura, and Y. Koide, J. J. Appl. Phys. **56** (2), 024101 (2017).
[91] M. J. Burek, D. Ramos, P. Patel, I. W. Frank, and M. Lončar, Appl. Phys. Lett. **103** (13), 131904 (2013).
[92] Y. Tao and C. Degen, Adv. Mater. **25** (29), 3962 (2013).
[93] Y. Tao, J. M. Boss, B. Moores, and C. L. Degen, Nat. Commun. **5** (1), 1 (2014).
[94] M. Liao, M. Toda, L. Sang, S. Hishita, S. Tanaka, and Y. Koide, Appl. Phys. Lett. **105** (25), 251904 (2014).
[95] J. Atulasimha and A. B. Flatau, Smart Mater. Struct. **20** (4), 043001 (2011).
[96] R. R. Basantkumar, B. Stadler, W. P. Robbins, and E. Summers, presented at the Magnetics Conference, 2006. INTERMAG 2006. IEEE International, 2006.
[97] P. Zhao, Z. Zhao, D. Hunter, R. Suchoski, C. Gao, S. Mathews, M. Wuttig, and I. Takeuchi, Appl. Phys. Lett. **94** (24), 243507 (2009).
[98] Z. Zhang, L. Sang, J. Huang, W. Chen, L. Wang, Y. Takahashi, S. Mitani, Y. Koide, S. Koizumi, and M. Liao, Carbon **170**, 294 (2020).
[99] Z. Zhang, G. Chen, K. Gu, S. Koizumi, and M. Liao, Functional Diamond **3** (1), 2221280 (2023).
[100] Z. Zhang, L. Sang, J. Huang, L. Wang, S. Koizumi, and M. Liao, J. Alloys Compd. **858**, 157683 (2021).
[101] H. A. Tilmans, M. Elwenspoek, and J. H. Fluitman, Sens. Actuat. A: Phys. **30** (1-2), 35 (1992).
[102] M. Imboden and P. Mohanty, Phys. Rep. **534** (3), 89 (2014).
[103] R. C. O'handley, Modern Magn. Mater. (2000).
[104] Y. Varshni, Phys. Rev. B **2** (10), 3952 (1970).
[105] S. C. Lakkad, J. Appl. Phys. **42** (11), 4277 (1971).
[106] J. Wachtman Jr, W. Tefft, D. Lam Jr, and C. Apstein, Phys. Rev. **122** (6), 1754 (1961).
[107] M. Toda, N. Inomata, T. Ono, and I. Voiculescu, IEEJ T Electr. Electr. **12** (2), 153 (2017).
[108] I. Voiculescu, M. Liao, M. Zakerin, R. Berger, T. Ono, and M. Toda, Sens. Actuat. A: Phys. **271**, 356 (2018).

[109] J. Reermann, G. Schmidt, S. Zabel, and F. Faupel, Procedia Eng. **120**, 536 (2015).
[110] B. Bahreyni and C. Shafai, IEEE Sen. J. **7** (9), 1326 (2007).
[111] W. Zhang and J. E.-Y. Lee, Sen. Actuat. A Phys. **211**, 145 (2014).
[112] M. Li, S. Nitzan, and D. A. Horsley, IEEE Electr. Dev. Lett. **36** (1), 62 (2014).
[113] M. A. Indianto, M. Toda, and T. Ono, Sen. Actuat. A Phys. **331**, 112985 (2021).
[114] S. Bennett, J. Baldwin, M. Staruch, B. Matis, J. LaComb, O. J. van't Erve, K. Bussmann, M. Metzler, N. Gottron, and W. Zappone, Appl. Phys. Lett. **111** (25), 252903 (2017).
[115] B. B. Pant, L. Withanawasam, M. Bohlinger, M. Larson, and B. W. Ohme, Additional Conferences (Device Packaging, HiTEC, HiTEN, & CICMT) **2015** (HiTEN), 000236 (2015).
[116] R. S. Popovic, presented at the 2014 29th International Conference on Microelectronics Proceedings-MIEL 2014, 2014.
[117] T. Yamamura, D. Nakamura, M. Higashiwaki, T. Matsui, and A. Sandhu, J. Appl. Phys. **99** (8), 08B302 (2006).
[118] T. Ciuk, B. Stanczyk, K. Przyborowska, D. Czolak, A. Dobrowolski, J. Jagiello, W. Kaszub, M. Kozubal, R. Kozlowski, and P. Kaminski, IEEE Trans. Electron Devices **66** (7), 3134 (2019).
[119] D. Rühmer, S. Bögeholz, F. Ludwig, and M. Schilling, Sens. Actuat. A Phys. **228**, 118 (2015).